

Discovery of Five Candidate Analogs for η Carinae in Nearby Galaxies

Rubab Khan^{1,2,5}, Scott M. Adams³, K. Z. Stanek^{3,4}, C. S. Kochanek^{3,4}, G. Sonneborn²

ABSTRACT

The late-stage evolution of very massive stars such as η Carinae may be dominated by episodic mass ejections which may later lead to Type II superluminous supernova (SLSN-II; e.g., SN 2006gy). However, as long as η Car is one of a kind, it is nearly impossible to quantitatively evaluate these possibilities. Here we announce the discovery of five objects in the nearby ($\sim 4 - 8$ Mpc) massive star-forming galaxies M 51, M 83, M 101 and NGC 6946 that have optical through mid-IR photometric properties consistent with the hitherto unique η Car. The *Spitzer* mid-IR spectral energy distributions of these $L_{bol} \simeq 3 - 8 \times 10^6 L_{\odot}$ objects rise steeply in the $3.6 - 8 \mu\text{m}$ bands, then turn over between 8 and $24 \mu\text{m}$, indicating the presence of warm ($\sim 400 - 600$ K) circumstellar dust. Their optical counterparts in HST images are $\sim 1.5 - 2$ dex fainter than their mid-IR peaks and require the presence of $\sim 5 - 10 M_{\odot}$ of obscuring material. Our finding implies that the rate of η Car-like events is a fraction $f = 0.094$ ($0.040 < f < 0.21$ at 90% confidence) of the core-collapse supernova (ccSN) rate. If there is only one eruption mechanism and SLSN-II are due to ccSN occurring inside these dense shells, then the ejection mechanism is likely associated with the onset of carbon burning ($\sim 10^3 - 10^4$ years) which is also consistent with the apparent ages of massive Galactic shells.

Subject headings: stars: evolution, massive, mass-loss — stars: individual (η Carinae)

1. Introduction

The last stages of the evolution of the most massive ($M \gtrsim 30 M_{\odot}$) stars may be dominated by episodic large mass-ejections (e.g., Humphreys & Davidson 1984; Smith 2014). This leads to dust

¹NASA Goddard Space Flight Center, MC 665, 8800 Greenbelt Road, Greenbelt, MD 20771; rubab.m.khan, george.sonneborn-1@nasa.gov

²NASA Postdoctoral Program, ORAU, P.O. Box 117, MS 36, Oak Ridge, TN 37831

³Dept. of Astronomy, The Ohio State University, 140 W. 18th Ave., Columbus, OH 43210; sadams, kstanek, ckochanek@astronomy.ohio-state.edu

⁴Center for Cosmology and AstroParticle Physics, The Ohio State University, 191 W. Woodruff Ave., Columbus, OH 43210

⁵JWST Fellow

condensing out of the ejecta, obscuring the star in the optical but revealing it in the mid-infrared (mid-IR) as the absorbed UV and optical photons are re-emitted at longer wavelengths (e.g., Kochanek et al. 2012). The best known example is η Carinae (η Car) which contains one of the most massive (100-150 M_{\odot}) and most luminous ($\sim 5 \times 10^6 L_{\odot}$) stars in our Galaxy (e.g., Robinson et al. 1973). Its Great Eruption in the mid-1800s led to the ejection of $\sim 10M_{\odot}$ of material (Smith et al. 2003) now seen as a dusty nebula around the star. While ongoing studies are helping us further analyze the Great Eruption (see, e.g., Rest et al. 2012; Prieto et al. 2014), deciphering the rate of such events and their consequences is challenging because no analog of this extraordinary laboratory for stellar astrophysics (in terms of stellar mass, luminosity, ejecta mass, time since mass ejection etc.) has previously been found.

A related puzzle is the existence of the Type II superluminous supernovae (SLSN-II) that are plausibly explained by the SN ejecta colliding with a massive shell of previously ejected material (e.g., SN 2006gy; Smith et al. 2007). A number of SNe, such as the Type Ib SN 2006jc (Pastorello et al. 2007) and the Type IIIn SN 2009ip (e.g., Mauerhan et al. 2012; Prieto et al. 2012; Pastorello et al. 2013), have also shown transients that could be associated with mass ejections shortly prior to the final explosion. But the relationship between these transients and η Car or other LBVs surrounded by still older, massive dusty shells (e.g., Smith & Owocki 2006) is unclear.

There are presently no clear prescriptions for how to include events like the Great Eruption into theoretical models. Even basic assumptions — such as whether the mass loss is triggered by the final post-carbon ignition phase as suggested statistically by Kochanek et al. (2012) or by an opacity phase-transition in the photosphere (e.g., Vink et al. 1999) or by interactions with a binary companion (e.g., Soker 2005) — are uncertain. Studies of possible mass-loss mechanisms (e.g., Shiode & Quataert 2014) are unfortunately non-prescriptive on either rate or outcome. Observationally, we are limited by the small numbers of high mass stars in this short evolutionary phase and searching for them in the Galaxy is complicated by having to look through the crowded, dusty disk and distance uncertainties. Obtaining a better understanding of this phase of evolution requires exploring other galaxies.

We demonstrated in Khan et al. (2010, 2011, 2013) that searching for extragalactic self-obscured stars utilizing *Spitzer* images is feasible, and in Khan et al. (2015a) we isolated an emerging class of 18 candidate self-obscured stars with $L_{bol} \sim 10^{5.5-6.0} L_{\odot}$ ($M_{ZAMS} \simeq 25-60M_{\odot}$) in galaxies at $\sim 1-4$ Mpc. We have now expanded our search to the large star-forming galaxies M 51, M 83, M 101 and NGC 6946 (distance $\simeq 4-8$ Mpc). We picked these galaxies because they have high star formation rates (total $SFR_{H\alpha} \simeq 6.9M_{\odot}/\text{yr}$, mainly based on Kennicutt et al. 2008) and hosted significant numbers of core-collapse supernovae (ccSNe) over the past century (total 20, e.g., Botticella et al. 2012), indicating that they are likely to host a significant number of evolved high mass stars.

In this letter, we announce the discovery of five objects in these galaxies that have optical through mid-IR photometric properties consistent with the hitherto unique η Car as it is presently observed. In what follows, we describe our search method (Section 2), analyze the physical prop-

erties of the five potential η Car analogs (Section 3) and consider the implications of our findings (Section 4).

2. The η Car Analog Candidates

At extragalactic distances, an η Car analog would appear as a bright, red point-source in *Spitzer* IRAC (Fazio et al. 2004) images, with a fainter optical counterpart due to self-obscuration. Given enough absorption, the optical counterpart could be undetectable. Building on our previous work (Khan et al. 2011, 2013, 2015a,b), we relied on these properties to identify the η Car analog candidates. For M 51 ($D \simeq 8$ Mpc, Ferrarese et al. 2000), M 83 ($D \simeq 4.61$ Mpc, Saha et al. 2006) and M 101 ($D \simeq 6.43$ Mpc, Shappee & Stanek 2011) we used the full *Spitzer* mosaics available from the Local Volume Legacy Survey (LVL, Dale et al. 2009), and for NGC 6946 ($D \simeq 5.7$ Mpc, Sahu et al. 2006) we used those from the *Spitzer* Infrared Nearby Galaxies Survey (SINGS, Kennicutt et al. 2003).

We built Vega-calibrated IRAC 3.6 – $8 \mu\text{m}$ and MIPS (Rieke et al. 2004) $24 \mu\text{m}$ point-source catalogs for each galaxy following the procedures described in Khan et al. (2015b). We use PSF photometry at 3.6 and $4.5 \mu\text{m}$, a combination of PSF and aperture photometry (preferring PSF) at $5.8 \mu\text{m}$, and only aperture photometry at 8.0 and $24 \mu\text{m}$ as the PSF size and PAH emission both increase toward longer wavelengths. For all sources, we determine the spectral energy distribution (SED) slope a ($\lambda L_\lambda \propto \lambda^a$), the total IRAC luminosity (L_{mIR}) and the fraction f of L_{mIR} that is emitted in the first three IRAC bands. Following the selection criteria established in Khan et al. (2013) — $L_{mIR} > 10^5 L_\odot$, $a > 0$ and $f > 0.3$ — we initially selected ~ 700 sources from our mid-IR point-source catalogs.

We examined the IRAC images to exclude the sources associated with saturated, resolved or foreground objects, and utilized the VizieR¹ web-service to rule out spectroscopically confirmed non-stellar sources and those with high proper motions. We inspected the 3.6 – $24 \mu\text{m}$ SEDs of the remaining sources to identify the ones that most closely resemble the SED of η Car and then queried the Hubble Source Catalog (HSC², Version 1) to exclude those with bright optical counterparts ($m \lesssim 20$ mag, implying $L_{opt} \gtrsim 1.5 - 6 \times 10^5 L_\odot$). These steps produced a short-list of ~ 20 sources for which we retrieved archival HST images and the associated photometry from the Hubble Legacy Archive (HLA³). Since the HST and *Spitzer* images sometimes have significant ($\sim 1''0$) astrometric mismatches, we utilized the IRAF GEOMAP and GEOXYTRAN tasks to locally align the HST and *Spitzer* images with uncertainties $\lesssim 0''.1$. We then searched for the closest optical counterpart within a matching radius of $0''.3$.

¹<http://vizier.u-strasbg.fr/>

²<https://archive.stsci.edu/hst/hsc/search.php>

³<http://hla.stsci.edu/>

We identified five sources with mid-IR SEDs closely resembling that of η Car and optical fluxes or flux limits $\sim 1.5 - 2$ dex fainter than their mid-IR peaks. We will refer to these sources as η Twins-1, 2, 3, 4 and 5. We find one source each in M 51 (η Twin-1), M 101 (η Twin-2) and NGC 6946 (η Twin-3), and two sources in M 83 (η Twins-4, 5). We identified HST counterparts of η Twins-1, 2 and 4 within the $0''.3$ matching radius. For η Twin-3, no HST source is cataloged within the matching radius, so we visually identified the closest location of flux excess at $\sim 0''.3$, and used simple aperture photometry techniques to measure the I -band flux and the B and V band flux upper limits. For η Twin-5, although a cataloged HST source exists within the $0''.3$ matching radius, we selected a different source at $0''.35$ as the more likely photometric match because it is also a bright HST J -band source. Table 1 lists the photometry of these sources, Figure 1 shows their IRAC $3.6 \mu\text{m}$ and HST I -band images, and Figure 2 shows their SEDs. η Twins-1, 4 and 5 are $\text{H}\alpha$ emitters and η Twin-2 is a UV source (see Table 1).

We have $UBVR$ variability data for M 51, M 101 and NGC 6946 from the LBC survey for failed supernovae (Gerke et al. 2014). We analyzed 21/26/37 epochs of data spanning a 7.1/7.2/8 year period for M 51/M 101/NGC 6946 with the ISIS image subtraction package (Alard & Lupton 1998). We did not detect any significant optical variability at the locations of η Twins-1, 2 or 3.

Cutri et al. (2012) identified η Twin-2 as a WISE point source and we use their $12 \mu\text{m}$ flux measurement as an upper limit for SED models (Section 3). Johnson et al. (2001) reports an optically thick free-free radio source located $0''.49$ from η Twin-3 and Hadfield et al. (2005) identified a source with Wolf-Rayet spectroscopic signature $1''.54$ from η Twin-4. We could not confirm if these sources are reasonable astrometric matches to the IRAC locations. η Twins-4 and 5 were cataloged by Williams et al. (2015) but not flagged as massive stars.

3. SED Modeling

We fit the SEDs of these five sources using DUSTY (Ivezic & Elitzur 1997) to model radiation transfer through a spherical medium surrounding a blackbody source, which is also a good approximation for a combination of unresolved non-spherical/patchy/multiple circumstellar shells. We considered models with either graphitic or silicate dust (Draine & Lee 1984). The models are defined by the stellar luminosity (L_*), stellar temperature (T_*), V -band optical depth (τ_V), dust temperature at the inner-edge of the shell (T_d) and shell thickness $\zeta = R_{out}/R_{in}$. We embedded DUSTY inside a Markov Chain Monte Carlo (MCMC) driver to fit each SED by varying T_* , τ_V , and T_d with L_* determined by a χ^2 fit for each model. We fix $\zeta = 4$ since its exact value has little effect on the results (Khan et al. 2015a), limit T_* to a maximum value of $\sim 50,000$ K, set the minimum flux uncertainty to $\sim 10\%$ (0.1 magnitude) and do not account for distance uncertainties.

The best fit model parameters determine the radius of the inner edge of the stellar-ejecta distribution (R_{in}). The mass of the shell is $M_e = 4\pi R_{in}^2 \tau_V / \kappa_V$ (scaled to a visual opacity of $\kappa_V = 100 \kappa_{v100} \text{ cm}^2/\text{g}$) and the age estimate for the shell is $t_e = R_{in}/v_e$ (scaled as $v_e = 100 v_{e100} \text{ km s}^{-1}$)

where we can ignore R_{out} to zeroth order. Table 2 reports the parameters of the best fit models and Figure 2 shows these models. The integrated luminosity estimates depend little on the choice of dust type, and are in the range of $L_* \simeq 10^{6.5-6.9} L_\odot$. We also fit the SEDs using Castelli & Kurucz (2004) stellar atmosphere models instead of blackbodies. Since these resulted in similar parameter estimates, we only report the blackbody results.

Generally, the best fits derived for graphitic dust require lower optical depths, lower dust temperatures and larger shell radii, leading to higher ejecta masses and age estimates. For η Twins-2 and 4, the stellar temperature estimates reach the allowed maximum of $\sim 50,000$ K. The best fit models of η Twin-1 and 5 also require the presence of a hot star, but with temperatures lower than the allowed maximum ($\sim 27,600/37,750$ K and $\sim 23,500/37,500$ K for graphitic/silicate dust). Constrained by the low optical flux, the best fit models of η Twin-3 require the presence of a cool star ($\sim 5,000$ K). For η Twins-2, 4 and 5, the best fits derived for graphitic dust had lower χ^2 , and for η Twins-1 and 3 the best fits derived for silicate dust have lower χ^2 . Considering these models, the η Car analog candidates appear to be embedded in $\sim 5-10 M_\odot$ of warm ($\sim 400-600$ K) obscuring material ejected a few centuries ago.

Figure 3 contrasts the bolometric luminosities and ejecta mass estimates of these five objects with the relatively less luminous sources we identified in Khan et al. (2015a). The five new sources form a distinct cluster close to η Car in the $L_{bol} - M_{ejecta}$ parameter space, whereas the previously identified dusty-star candidates from Khan et al. (2015a) are more similar to the Galactic OH/IR star IRC+10420 (e.g., Tiffany et al. 2010) or M 33’s Variable A (e.g., Humphreys et al. 1987).

4. Discussion

To an extragalactic observer located in one of the targeted galaxies surveying the Milky Way with telescopes similar to the HST and *Spitzer*, η Car’s present day SED would appear nearly identical to the extragalactic η Car analog candidates we found. The Carina nebula is $\sim 2.5^\circ$ in extent (Smith & Brooks 2007) corresponding to $\sim 2''.5$ at our most distant galaxy (M 51 at 8 Mpc). While this would not be resolved by *Spitzer*, it would be easily resolved by HST. Because more compact clusters are not uncommon, in Khan et al. (2013) we considered whether dusty clusters can hide η Car like stars and if we would confuse unresolved star-clusters with η Car analogs. In general, a cluster sufficiently luminous to hide an evolved $\gtrsim 30 M_\odot$ star has hosted many luminous stars with strong UV radiation fields and winds, which will generally clear the cluster of the gas and dust needed to produce strong mid-IR emission over the timescale that even the most massive star needs to evolve away from the main sequence. Moreover, emission from warm circumstellar ejecta peaks between the IRAC $8 \mu\text{m}$ and MIPS $24 \mu\text{m}$ bands and then turns over, as seen in all of our candidates, unlike emission from colder intra-cluster dust that generally peaks at longer wavelengths.

A significant majority of massive stars are expected to be in multiple-star systems (e.g.,

Sana & Evans 2011), as is the case for η Car (e.g., Daminieli 1996; Mehner et al. 2010). This is a minor complication, affecting luminosity estimates by at most a factor of 2, and mass estimates even less. Assuming all the candidates we have identified are real analogs of η Car, then our galaxy sample (including the Milky Way) contains $N_c = 6$ η Car-like stars. Based on the ratio of star formation rates (2 vs. $10M_\odot/\text{yr}$), our original sample of 7 galaxies would be expected to have ~ 1 η Car analog, which is statistically consistent with not finding one in Khan et al. (2015a).

If we expand our simple rate estimates from Khan et al. (2015a), our $N_c = 6$ sources implies an eruption rate over the 12 galaxies (7 previous, 4 in this work, and the Milky Way) of $F_e = 0.033t_{d200}^{-1}\text{yr}^{-1}$ ($0.016\text{yr}^{-1} < F_e t_{d200} < 0.059\text{yr}^{-1}$ at 90% confidence) where $t_d \simeq 200$ yrs is a rough estimate of the period over which our method would detect an η Car-like source. For comparison, the number of ccSN recorded in these galaxies over the past 30 years is 10 (mainly based on Botticella et al. 2012) for an SN rate of $F_{SN} = 0.33/\text{yr}$. This implies that the rate of η Car-like events is a fraction $f = 0.094$ ($0.040 < f < 0.21$ at 90% confidence) of the ccSNe rate.

If there is only one eruption mechanism and the SLSN-II are due to ccSN occurring inside these dense shells, then the ratio of the rate of η Car-like events and SLSN-II, $r_{SLSN}/r_\eta = t_{SLSN}/t_\eta$, is the ratio of the time period t_{SLSN} during which the shell is close enough to the star to cause a SLSN to the time period t_η over which shell ejections occur. With $r_{SLSN} \sim 10^{-3}$ of the core-collapse rate (Quimby et al. 2013), we must have that $t_{SLSN}/t_\eta \sim 10^{-2}$. A typical estimate is that $t_{SLSN} \sim 10$ to 10^2 years, which implies $t_\eta \sim 10^3$ to 10^4 years, consistent with the properties of the massive shells around luminous stars observed in our own Galaxy and suggesting that the instabilities driving the eruptions are linked to the onset of carbon burning (Kochanek 2011). This would also imply the existence of “superluminous” X-ray ccSN, where an older shell of material is too distant and low density to thermalize the shock heated material but is still dense enough for the cooling time to be faster than the expansion time. Such events should be ~ 10 times more common than optical SLSN-II. If the eruptions driving SLSN-II are only associated with later and shorter burning phases (e.g., as in Shiode & Quataert 2014) then there must be two eruption mechanisms and the vast majority of η Car analogs will not be associated with the SLSN-II mechanism.

We identified the 5 potential η Car analogs by specifically focusing on finding sources that most closely resemble the SED of present day η Car. The reason that the SEDs of these five sources are so remarkably similar to each other is by design. We have not closely studied the less luminous mid-IR sources that may belong to the class of candidate self-obscured stars we identified in Khan et al. (2015a), and some of the sources that we excluded because they have relatively bright optical counterparts may be evolved high mass stars with older, lower optical-depth shells. It is readily apparent that a closer scrutiny of our mid-IR catalogs should reveal richer and more diverse populations of evolved massive stars. This in turn will let us better quantify the abundance of those stars, and constrain the rates of mass ejection episodes and mass loss from massive stars prior to their death by core-collapse.

The η Car analog candidates we identified can be studied at greater detail with the James Webb

Space Telescope (JWST, e.g., Gardner et al. 2006), taking advantage of its order-of-magnitude-higher spatial resolution. These sources are luminous in the $3.6 - 24 \mu\text{m}$ wavelength range where the JWST will be most sensitive. They are rare laboratories for stellar astrophysics and will be very interesting extragalactic stellar targets for spectroscopic study with JWST’s mid-IR instrument (MIRI, Rieke et al. 2015). This will give us an unprecedented view of these most-massive self-obscured stars, letting us study their evolutionary state and the composition of their circumstellar ejecta.

We thank the referee for helpful comments. RK is supported by a JWST Fellowship awarded through the NASA Postdoctoral Program. SMA is supported by a Presidential Fellowship at The Ohio State University. KZS is supported in part by NSF Grant AST-151592. CSK is supported by NSF grant AST-1515876. This research has made use of observations made with the *Spitzer* Space Telescope, which is operated by the JPL and Caltech under a contract with NASA; observations made with the NASA/ESA Hubble Space Telescope and obtained from the Hubble Legacy Archive, which is a collaboration between the STScI/NASA, ST-ECF/ESA and the CADC/NRC/CSA; and the VizieR catalog access tool, CDS, Strasbourg, France.

REFERENCES

- Alard, C. & Lupton, R. H. 1998, *ApJ*, 503, 325
- Botticella, M. T., Smartt, S. J., Kennicutt, R. C., et al. 2012, *A&A*, 537, A132
- Castelli, F., & Kurucz, R. L. 2004, arXiv:astro-ph/0405087
- Cutri, R. M. et al. 2012, VizieR Online Data Catalog, 2311, 0
- Dale, D. A. et al. 2009, *ApJ*, 703, 517
- Damineli, A. 1996, *ApJ*, 460, L49
- Draine, B. T. & Lee, H. M. 1984, *ApJ*, 285, 89
- Fazio, G. G. et al. 2004, *ApJS*, 154, 10
- Ferrarese, L., Mould, J. R., Kennicutt, R. C., Jr., et al. 2000, *ApJ*, 529, 745
- Gardner, J. P. et al. 2006, *SSR*, 123, 485
- Gerke, J. R., Kochanek, C. S., & Stanek, K. Z. 2015, *MNRAS*, 450, 3289
- Hadfield, L. J., Crowther, P. A., Schild, H., & Schmutz, W. 2005, *A&A*, 439, 265
- Humphreys, R. M. & Davidson, K. 1984, *Science*, 223, 243

- Humphreys, R. M., Jones, T. J., & Gehrz, R. D. 1987, *AJ*, 94, 315
- Ivezic, Z. & Elitzur, M. 1997, *MNRAS*, 287, 799
- Johnson, K. E., Kobulnicky, H. A., Massey, P., & Conti, P. S. 2001, *ApJ*, 559, 864
- Kennicutt, Jr., R. C. et al. 2003, *PASP*, 115, 928
- . 2008, *ApJS*, 178, 247
- Khan, R. et al. 2010, *ApJ*, 715, 1094
- Khan, R., Stanek, K. Z., Kochanek, C. S., & Bonanos, A. Z. 2011, *ApJ*, 732, 43
- Khan, R., Stanek, K. Z., & Kochanek, C. S. 2013, *ApJ*, 767, 52
- Khan, R., Kochanek, C. S., Stanek, K. Z., & Gerke, J. 2015a, *ApJ*, 799, 187
- Khan, R., Stanek, K. Z., Kochanek, C. S., & Sonneborn, G. 2015b, *ApJS*, 219, 42
- Kochanek, C. S. 2011, *ApJ*, 743, 73
- Kochanek, C. S., Szczygieł, D. M., & Stanek, K. Z. 2012, *ApJ*, 758, 142
- Mauerhan, J. C., Smith, N., Filippenko, A. V., et al. 2013, *MNRAS*, 430, 1801
- Mehner, A., Davidson, K., Ferland, G. J., & Humphreys, R. M. 2010, *ApJ*, 710, 729
- Pastorello, A. et al. 2007, *Nature*, 447, 829
- Pastorello, A., Cappellaro, E., Inserra, C., et al. 2013, *ApJ*, 767, 1
- Prieto, J. L., Brimacombe, J., Drake, A. J., & Howerton, S. 2013, *ApJ*, 763, L27
- . 2014, *ApJ*, 787, L8
- Quimby, R. M., Yuan, F., Akerlof, C., & Wheeler, J. C. 2013, *MNRAS*, 431, 912
- Rest, A., Prieto, J. L., Walborn, N. R., et al. 2012, *Nature*, 482, 375
- Rieke, G. H. et al. 2004, *ApJS*, 154, 25
- Rieke, G. H., Wright, G. S., Böker, T., et al. 2015, *PASP*, 127, 584
- Robinson, G., Hyland, A. R., & Thomas, J. A. 1973, *MNRAS*, 161, 281
- Saha, A. et al. 2006, *ApJS*, 165, 108
- Sahu, D. K. et al. 2006, *MNRAS*, 372, 1315
- Sana, H., & Evans, C. J. 2011, *IAU Symposium*, 272, 474

- Shappee, B. J., & Stanek, K. Z. 2011, *ApJ*, 733, 124
- Shiode, J. H., & Quataert, E. 2014, *ApJ*, 780, 96
- Smith, N., Gehrz, R. D., Hinz, P. M., et al. 2003, *AJ*, 125, 1458
- Smith, N. & Owocki, S. P. 2006, *ApJ*, 645, L45
- Smith, N. & Brooks, K. J. 2007, *MNRAS*, 379, 1279
- Smith, N., Li, W., Foley, R. J., et al. 2007, *ApJ*, 666, 1116
- Smith, N. 2014, *ARA&A*, 52, 487
- Soker, N. 2005, *ApJ*, 619, 1064
- Tiffany, C., Humphreys, R. M., Jones, T. J., & Davidson, K. 2010, *AJ*, 140, 339
- Vink, J. S., de Koter, A., & Lamers, H. J. G. L. M. 1999, *A&A*, 350, 181
- Williams, S. J., Bonanos, A. Z., Whitmore, B. C., Prieto, J. L., & Blair, W. P. 2015, *A&A*, 578, A100

Table 1: Multi-Wavelength Photometry

	η Twin-1	η Twin-2	η Twin-3	η Twin-4	η Twin-5
Host	M 51	M 101	NGC 6946	M 83	M 83
RA (deg)	202.46287	210.80203	308.76548	204.21782	204.21523
Dec (deg)	47.21126	54.31891	60.18314	-29.88722	-29.87481
m_{UV}	...	23.25 ± 0.05
m_U	24.34	23.16 ± 0.03	...	22.27 ± 0.02	22.84 ± 0.04
m_B	25.14	24.26 ± 0.03	> 26.70	23.31 ± 0.02	22.83 ± 0.02
m_V	23.64 ± 0.06	23.92 ± 0.03	> 26.15
$m_{H\alpha}$	18.26 ± 0.01	22.00 ± 0.06	22.14 ± 0.07
m_R	21.90 ± 0.03
m_I	22.31 ± 0.08	23.23 ± 0.03	24.56 ± 0.26	22.58 ± 0.03	21.84 ± 0.02
m_J	21.12 ± 0.07
m_H	19.14 ± 0.02
$m_{3,6}$	14.68 ± 0.12	15.08 ± 0.11	14.45 ± 0.11	14.26 ± 0.10	14.59 ± 0.12
$m_{4,5}$	14.10 ± 0.06	13.97 ± 0.04	14.20 ± 0.06	13.79 ± 0.07	14.30 ± 0.09
$m_{5,8}$	12.20 ± 0.05	11.99 ± 0.06	11.47 ± 0.09	11.40 ± 0.08	11.54 ± 0.09
$m_{8,0}$	10.38 ± 0.10	10.12 ± 0.01	9.84 ± 0.06	9.70 ± 0.11	9.95 ± 0.07
m_{12}	...	> 8.81
m_{24}	6.50 ± 0.20	7.07 ± 0.02	6.09 ± 0.13	6.09 ± 0.20	6.47 ± 0.05

Vega magnitudes of the sources where the specific HST filters are UV:F275W; U :F336W, B :F435W (η Twin-2) / F438W (4, 5) / F439W (1) / F450W (3); V :F555W, $H\alpha$:F656N (η Twin-1) / F657N (4, 5), R :F675W, I :F814W, J :F110W, H :F160W. The HLA catalog reports no uncertainties for the U/B magnitudes of η Twin-1. The HST data sources are: η Twin-1: Prop.ID 7375 (PI:Scoville) and Prop.ID 12490 (PI:Koda); η Twin-2: Prop.ID 9490 (PI:Kuntz) and Prop.ID 13364 (PI:Calzetti); η Twin-3: Prop.ID 9073 (PI:Bregman); η Twins-4, 5: Prop.ID 12513 (PI:Blair)

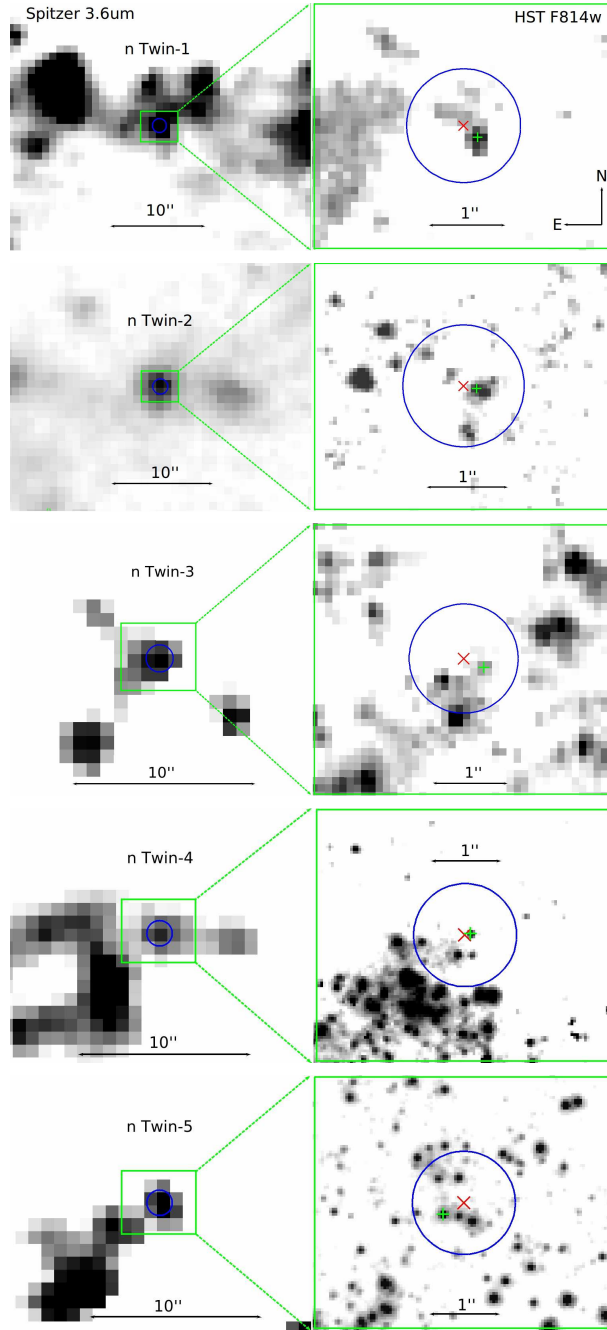


Fig. 1.— *Spitzer* IRAC $3.6\ \mu\text{m}$ (left column) and HST *I*-band (F814W, right column) images of the candidate η Car analogs. The HST images were taken with ACS (η Twin-1), WFPC2 (2, 3) and WFC3 (4, 5). The circles are $1''.5$ in diameter, which is roughly equal to the IRAC $3.6\ \mu\text{m}$ PSF FWHM. The rectangles on the left column enclose the regions shown on the right column. On the HST images, “ \times ” marks the location of the IRAC source (center of the circle) determined through pixel-to-pixel mapping and “ $+$ ” marks the location of the likely optical counterpart as discussed in Section 2.

Table 2: Best Fit SED Models

ID	$\chi^2/(m+n)$	τ_V	T_d (K)	T_* (K)	$\log(R_{in})$ (cm)	$\log L_{bol}$ (L_\odot)	M_e (M_\odot)	t_e (years)
<i>Graphitic</i>								
η Twin-1	151/(11 + 0)	4.34	386	27,610	17.53	6.842	32.04	1087
η Twin-2	92/(10 + 1)	2.51	404	50,120	17.37	6.554	8.81	750
η Twin-3	87/(6 + 2)	16.67	337	5,570	17.44	6.920	78.76	870
η Twin-4	113/(8 + 0)	2.24	394	50,110	17.39	6.544	8.59	783
η Twin-5	269/(9 + 0)	3.61	375	23,530	17.37	6.504	12.62	748
<i>Silicate</i>								
η Twin-1	130/(11 + 0)	6.34	603	37,740	16.97	6.890	3.53	299
η Twin-2	205/(10 + 1)	4.22	641	50,120	16.79	6.573	0.99	194
η Twin-3	69/(6 + 2)	34.30	424	4,730	16.71	6.839	5.78	164
η Twin-4	136/(8 + 0)	3.94	622	50,120	16.80	6.555	0.97	199
η Twin-5	307/(9 + 0)	4.57	760	37,520	16.59	6.449	0.44	124

The format $\chi^2/(m+n)$ indicates the goodness of fit χ^2 , the number of flux measurements m used to determine the luminosity and the number of upper limits n added to the estimate of χ^2 once the luminosity is determined.

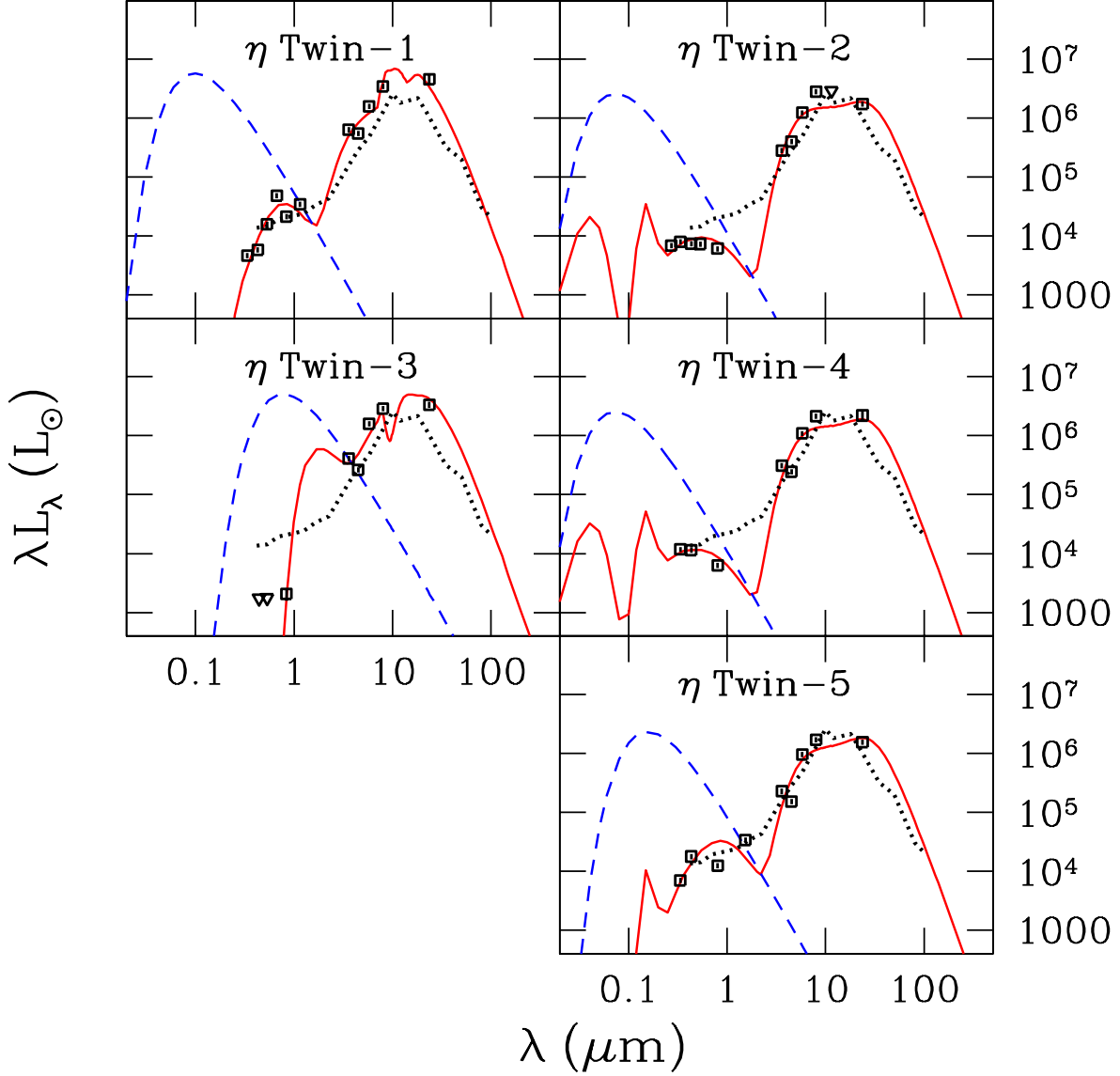


Fig. 2.— The best fit models (solid line) for the observed SEDs (squares and triangles with the latter for upper limits) of the candidate η Car analogs and the SEDs of the underlying, unobscured blackbody sources (dashed line), as compared to the SED of η Car (dotted line, from Robinson et al. 1973). The vertical bars show the larger of the flux uncertainties reported in Table 1 and the $\sim 10\%$ minimum flux uncertainty (0.1 magnitude) used for SED modeling (not accounting for distance uncertainties). Here we show the best fit silicate models for η Twins-1 and 3, and the best fit graphitic models for η Twins-2, 4 and 5.

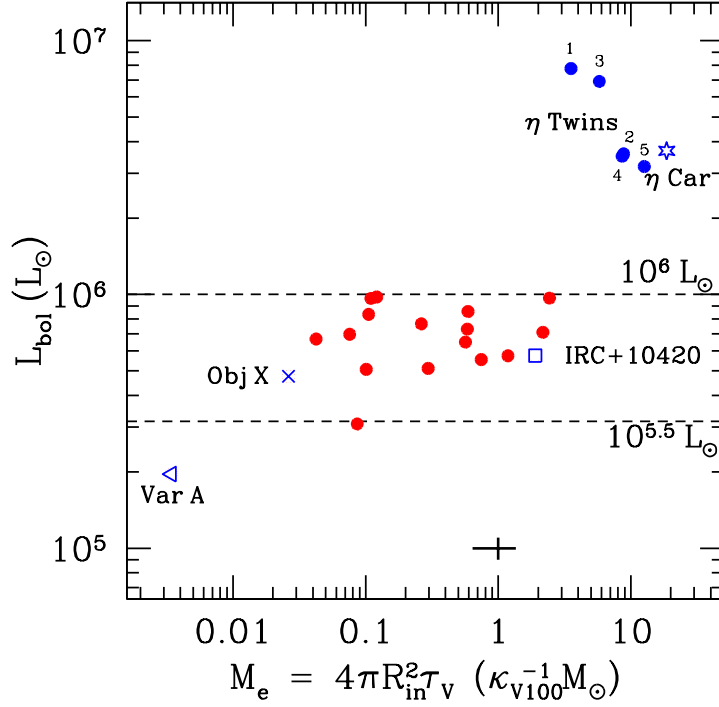


Fig. 3.— The luminosities, L_{bol} , of the candidate η Car analogs (blue circles) as a function of the ejecta mass estimates, $M_e = 4\pi R_{in}^2 \tau_V / \kappa_V$, compared to the less luminous (red circles) self-obscured star candidates we identified in Khan et al. (2015a). The Galactic OH/IR star IRC+10420 (e.g., Tiffany et al. 2010, square), M33’s Variable A (e.g., Humphreys et al. 1987, triangle), Object X (“x”, Khan et al. 2011) and η Car (star symbol) are also shown for comparison. The error bar corresponds to the typical 1σ uncertainties on L_{bol} ($\pm 10\%$) and M_e ($\pm 35\%$) of the best SED fit models.